EXTENDED PDF FORMAT
SPONSORED BY
Stem Cell Marker Antibodies
>Learn More
R&D SYSTEMS
www.rndsystems.com

Complex Dental Structure and Wear Biomechanics in Hadrosaurid Dinosaurs

Gregory M. Erickson *et al.*

Science **338**, 98 (2012);
DOI: 10.1126/science.1224495

This copy is for your personal, non-commercial use only.

If you wish to distribute this article to others, you can order high-quality copies for your colleagues, clients, or customers by clicking here.

Permission to republish or repurpose articles or portions of articles can be obtained by following the guidelines here.

The following resources related to this article are available online at www.sciencemag.org (this information is current as of July 5, 2013):

Updated information and services, including high-resolution figures, can be found in the online version of this article at:
http://www.sciencemag.org/content/338/6103/98.full.html

Supporting Online Material can be found at:
http://www.sciencemag.org/content/suppl/2012/10/03/338.6103.98.DC1.html
http://www.sciencemag.org/content/suppl/2012/10/03/338.6103.98.DC2.html

A list of selected additional articles on the Science Web sites **related to this article** can be found at:
http://www.sciencemag.org/content/338/6103/98.full.html#related

This article **cites 26 articles**, 6 of which can be accessed free:
http://www.sciencemag.org/content/338/6103/98.full.html#ref-list-1

This article appears in the following **subject collections:**
Paleontology
http://www.sciencemag.org/cgi/collection/paleo

Downloaded from www.sciencemag.org on July 5, 2013

Science (print ISSN 0036-8075; online ISSN 1095-9203) is published weekly, except the last week in December, by the American Association for the Advancement of Science, 1200 New York Avenue NW, Washington, DC 20005. Copyright 2012 by the American Association for the Advancement of Science; all rights reserved. The title *Science* is a registered trademark of AAAS.

Complex Dental Structure and Wear Biomechanics in Hadrosaurid Dinosaurs

Gregory M. Erickson,[1]* Brandon A. Krick,[2] Matthew Hamilton,[2] Gerald R. Bourne,[3] Mark A. Norell,[4] Erica Lilleodden,[5] W. Gregory Sawyer[2]

Mammalian grinding dentitions are composed of four major tissues that wear differentially, creating coarse surfaces for pulverizing tough plants and liberating nutrients. Although such dentition evolved repeatedly in mammals (such as horses, bison, and elephants), a similar innovation occurred much earlier (~85 million years ago) within the duck-billed dinosaur group Hadrosauridae, fueling their 35-million-year occupation of Laurasian megaherbivorous niches. How this complexity was achieved is unknown, as reptilian teeth are generally two-tissue structures presumably lacking biomechanical attributes for grinding. Here we show that hadrosaurids broke from the primitive reptilian archetype and evolved a six-tissue dental composition that is among the most sophisticated known. Three-dimensional wear models incorporating fossilized wear properties reveal how these tissues interacted for grinding and ecological specialization.

Hadrosaurids were the dominant large herbivores of Late Cretaceous Europe, Asia, and North America (*1*). Gut and fecal contents show that these gregarious, facultative bipeds (Fig. 1A) with broad ducklike bills grazed on horsetail, fern, and primitive angiosperm ground cover and browsed on conifers (*2*). These tough plants, laden with siliceous phytoliths and/or exogenous grit that scoured their teeth (*1*), were pulverized using dentitions consisting of columns of developing and functional teeth with flattened horse- and bison-like grinding surfaces (*3, 4*) (Fig. 1, B to D). It's likely that exploitation of these resources, which were presumably not as accessible to their forebears who had shearing teeth (*5*–*7*) (Fig. 1E), facilitated the extensive hadrosaurid radiation (*8, 9*).

The traditional model of hadrosaurid chewing surfaces includes only the primitive reptilian (Sauria) dental tissues enamel (hard hypermineralized material) and orthodentine ("dentine"; soft bonelike tissue) (*3, 4*) (Fig. 2A). Accordingly, file-like crests and basins would have formed on tooth surfaces because of differential wear resistance as the teeth moved across the chewing surface (*6*) (Fig. 1C).

This model contrasts with what we see in more complex mammalian grinding teeth (*10*–*14*) (Fig. 1D). In mammals, the major tissues, besides enamel and orthodentine, include soft secondary dentine (that forms a lower tier within basins, sealing the pulp cavity to prevent abscesses) and coronal cementum (a derived root attachment tissue that migrates onto the crowns, reducing stress on the brittle crests by transmitting loads among tissues).

The current model of hadrosaurid dental architecture is simplistic, lacking both crest-supporting and abscess-preventative tissues. Furthermore, enamel is present only in the leading teeth in the lower batteries (Fig. 2A), thereby leaving no hard tissues to form subsequent crests (Fig. 2B). Finally, conspicuous features are unaccounted for, including granular material between teeth and filling pits within basins, slicing planes on leading-edge teeth, and branched and linear ridges within the basins (*15*) (Fig. 2, B and C).

How was mammal-like grinding achieved in hadrosaurids? We provide answers by (i) characterizing tissue compositions and chewing surface morphologies in hadrosaurids and outgroups, (ii) mechanically testing the tissues for wear-relevant attributes, (iii) using those properties in a tribological (study of wear) model to reveal the biomechanics of grinding-surface formation, and (iv) summarizing these findings in an evolutionary context.

Comprehensive phylogenies for the Hadrosauridae (*8*) (fig. S1) and Ornithischia (*16*) were used to identify 27 taxa representing dental variation throughout the ornithopodan radiation (table S1). The tissue compositions were determined from intact batteries and transversely sectioned teeth using dissecting and/or polarizing microscopy (*17*). Casts of worn chewing surfaces were made and the morphologies digitally captured using laser scanning confocal

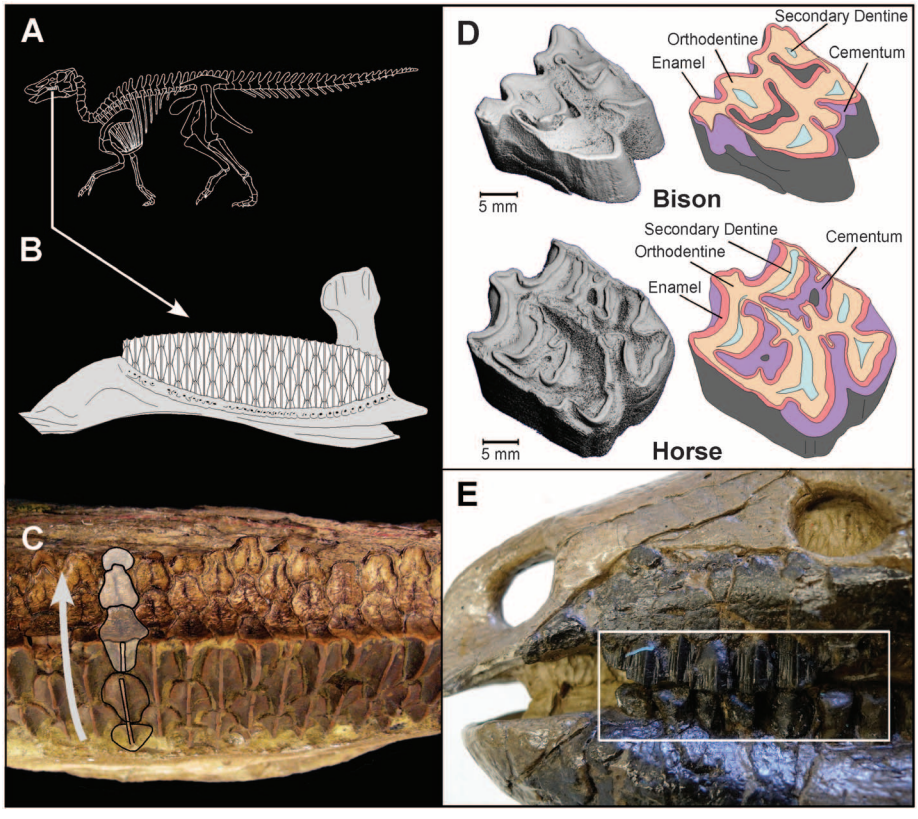

Fig. 1. Dental comparisons. (**A**) Hadrosaurid skeleton (*Edmontosaurus*). (**B**) Dental battery showing developing teeth (lingual view). (**C**) *Edmontosaurus* dental battery showing the progression of developing teeth and the grinding surface with teeth in various wear stages. (**D**) Ungulate grinding molars showing four-tissue composition. (**E**) Hadrosaurid outgroup condition (*Camptosaurus*) possessing individual shearing teeth at each position.

[1]Department of Biological Science, Florida State University, Tallahassee, FL 32306–4295, USA. [2]Department of Mechanical and Aerospace Engineering, University of Florida, Gainesville, FL 32611, USA. [3]Department of Metallurgical and Materials Engineering, Colorado School of Mines, Golden, CO 80401, USA. [4]Division of Paleontology, American Museum of Natural History, New York, NY 10024, USA. [5]Institute of Materials Research, Materials Mechanics, Helmholtz-Zentrum Geesthacht, Geesthacht, Germany.

*To whom correspondence should be addressed. E-mail: gerickson@bio.fsu.edu

Downloaded from www.sciencemag.org on July 5, 2013

microscopy and micro-computerized tomography (fig. S2).

Relative values for tissue wear rates (a direct measure of material removal) and hardnesses (the resistance of a solid to permanent deformation when loaded) are the most pertinent properties to determine how dental tissues contribute to whole-tooth abrasive wear (*18, 19*). Before this study, these had not been recovered from fossil teeth. In dried modern teeth, analogs to well-preserved fossils, material properties are commonly recovered (*20*), because apatite mineral content is the major determinant of osseous tissue hardness (*21*). In a feasibility analysis, we used nanoindentation hardness testing on extant and Late Pleistocene bison molar tissues, in which tissues were indented with a diamond tip with equal force to provide comparative data (*17*). This showed comparable relative values between the tissues of fossil and extant teeth (Fig. 3C).

We characterized the hadrosaurid tissue wear properties by subjecting an *Edmontosaurus* [American Museum of Natural History (AMNH) specimen no. 5896] dental battery to microtribological wear testing, in which a diamond-tipped probe was drawn across the tooth (at a sliding velocity of 1 mm/s, with 100 mN of normal force) to mimic abrasive feeding strokes (*17*) (fig. S4). A surface profiler measured the volume of material removed, which was divided by the product of the normal force and the sliding distance to reveal the wear rates (*17*). Indicators that biological values were recovered included the correspondence of wear depths to relief on naturally worn batteries, and the capacity to replicate the chewing surface topography using a three-dimensional tribological simulation (*17, 22*) based on Archard's wear law (*18, 23*) (Eq. 1)

$$V(\mathrm{mm}^3) = K[\mathrm{mm}^3/(\mathrm{Nm})]F_\mathrm{n}(\mathrm{N})d(\mathrm{m}) \quad (1)$$

{The volume of material lost, V (in mm^3), is equal to wear rate, K [in mm^3/(Nm)], times normal load, F_n (in newtons, N), times sliding distance, d (in meters, m).}

The model numerically simulates topographical changes to a multi-tissue hadrosaurid dental battery subjected to wear with an abrasive compliant pad analogous to hadrosaurid fodder. Starting from a planar surface encompassing tissue distributions and wear rates, the progressive coupling of wear and contact pressure (a function of surface geometry) results in an equilibrium topography where all tissues recede at equal rates. The model was ultimately used to test how tissue distributions act to create surface features through wear.

To confirm that wear-relevant properties are preserved in the 65- to 69-million-year-old fossils, we nanoindented teeth from AMNH 5896 and two others (*17*). Indicators for preservation include hardnesses correspondent with wear rates, similar values among individuals, and the capacity to predict the chewing surface morphology through the wear model, using hardness as a wear rate proxy (*17*). We also collected comparative data for the domestic horse (*Equus caballus*).

Results show that hadrosaurid teeth were composed of six major tissues (Fig. 2D). These include all four wear-relevant constituents that characterize mammalian grinding teeth: enamel and orthodentine, as well as independently derived secondary dentine and coronal cementum [a tissue used to demonstrate mammalian dental sophistication (*10*, *14*)]. Giant tubules (infilled pulp cavity branches) and a thick mantle dentine are also present. These results suggest that hadrosaurid teeth were among the most histologically complex of any animal. Additionally, unlike mammalian teeth (*11*), tissue distribution varied substantially within each tooth, exposing different configurations as they migrated across the chewing surface (Fig. 2, D and E). This allowed a single tooth to assume different forms and functions during its progression.

Tribology experiments revealed wear rates ranging from ~90 × 10^{-6} mm^3/Nm for orthodentine (the least wear-resistant) to ~6 × 10^{-6} mm^3/Nm

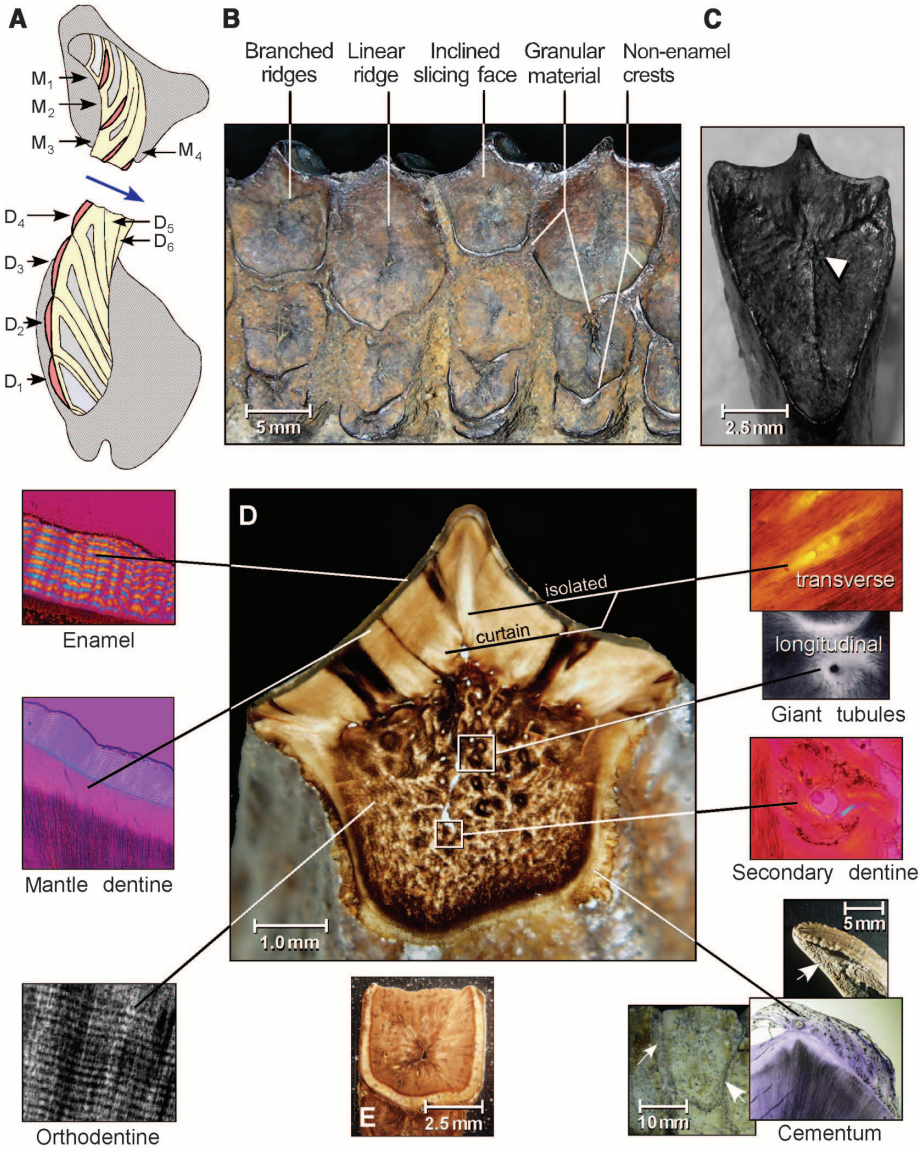

Fig. 2. Hadrosaurid dental organization. (**A**) Two-tissue model, frontal section of jaws depicting just enamel (red) and dentine (yellow) tooth composition (*3, 4*), with no enamel layers across the lower chewing surface. The upper (maxillary) teeth and lower (dentary) teeth were drawn at various angles across one another (*1*). The blue arrow depicts the movement of the upper teeth across the lower ones. The lower teeth may have been simultaneously drawn in the opposite direction. Tooth developmental stages are numbered in the upper ($M_\#$) and lower ($D_\#$) jaws. [Worn teeth were shed every 45 to 80 days from each column (*7*), up to 1880/year in total (*17*).] (**B**) Unexplained chewing surface features. (**C**) *Hadrosaurus* tooth with a Y-shaped ridge (arrow). (**D**) Sections through *Edmontosaurus* teeth showing tissues. Their presence and configurations vary throughout individual teeth. For instance, the roots (**E**), which become exposed, lack giant tubules. Coronal cementum (arrows) is present on the chewing surface and sides of a crown.

Downloaded from www.sciencemag.org on July 5, 2013

for enamel (the most wear-resistant) (Fig. 3, A, B, and D), which correspond to topographic features on worn batteries (Figs. 1C and 2B). Input of these values into the wear model resulted in a three-dimensional topography seen in naturally worn batteries. This includes crests where enamel is absent, as well as branched ridges (Fig. 4). Simulation reveals the contributions of each tissue to the worn topography (fig. S5). This shows that the overall morphology is impossible to achieve without the entire tissue ensemble (figs. S5 and S6). These findings

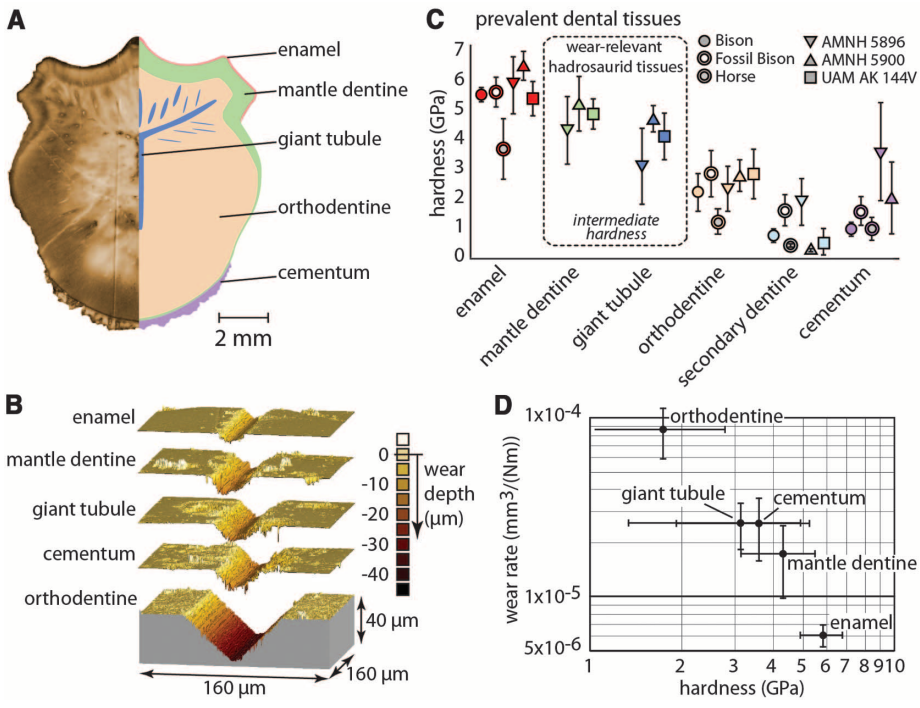

Fig. 3. Wear and hardness characterization. (**A**) Planarized *Edmontosaurus* tooth with wear track (left). (**B**) Profilometry of scratched tissues in AMNH 5896. Secondary dentine was not tested owing to its negligible footprint. (**C**) Mean and standard deviation from nanoindentation experiments on wear-relevant tissues in ungulates and hadrosaurids. The fossil bison absolute hardness values appear to be elevated from the degradation of elastic collagen, but the preservation of relative hardness, which is critical for understanding wear, is evident. Tissue-specific hardnesses in extant ungulate grinding teeth are highly variable among taxa. An exact match between values for the bison or horse and the analogous *Edmontosaurus* tissues is not expected. (**D**) Mean wear rates and standard deviation versus mean hardness and standard deviation for AMNH 5896 tissues.

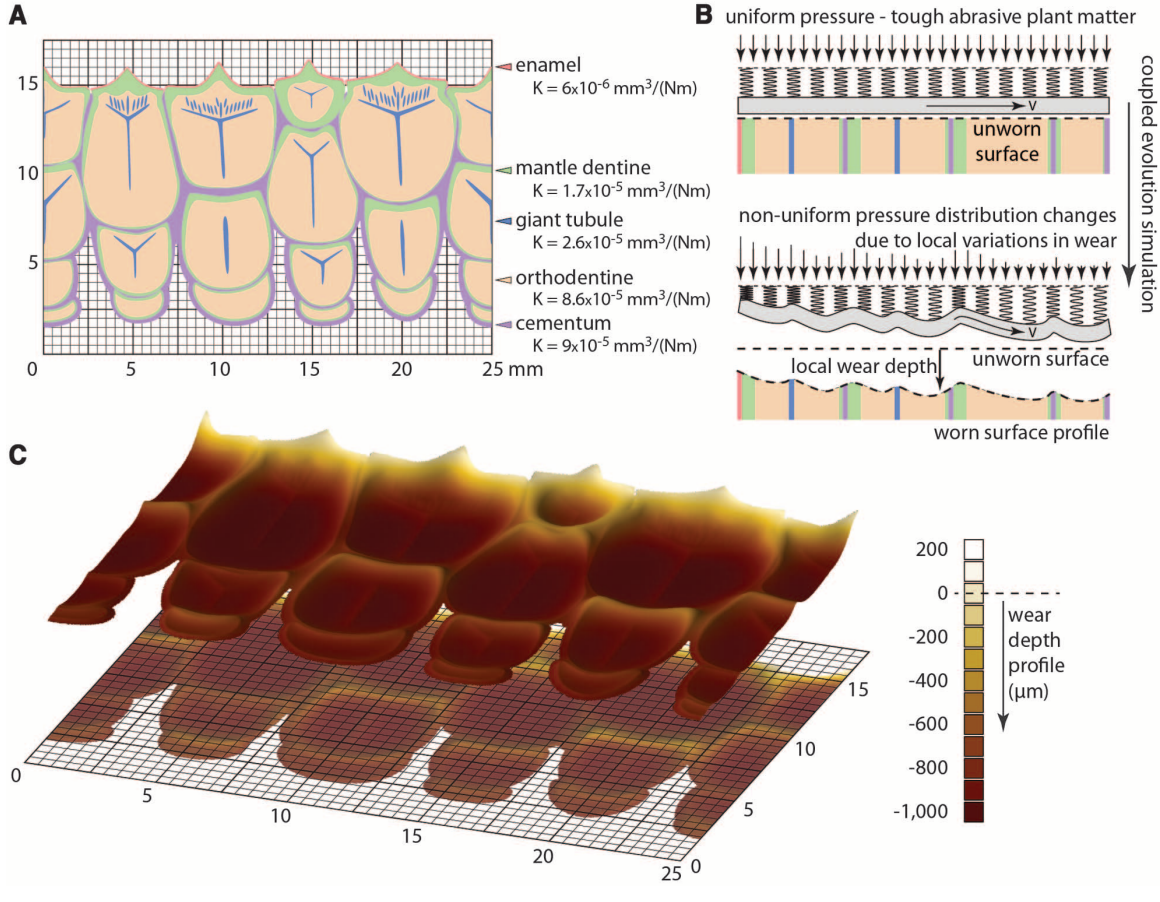

Fig. 4. Tribological modeling of the AMNH 5896 dental battery. (**A**) Tissue distribution and measured wear rates used in the simulation. (**B**) Schematic of the computational framework and simulation procedure. An initially flat composite is exposed to abrasive wear under uniform pressure. The progression of wear depth and contact pressure are linked, leading to uniform recession only at a steady state. (**C**) Equilibrium profile following computational wear modeling of an initially planar composite surface of varying tissue types assigned fossilized wear-rate values.

Downloaded from www.sciencemag.org on July 5, 2013

provide strong evidence that biologically relevant tribological properties are preserved in the fossil teeth.

Nanoindentation revealed mean hardness values from ~1 GPa for secondary dentine to ~6 GPa for enamel (Fig. 3C). Hardness and wear rates are related as expected for AMNH 5896 (Fig. 3D), and hardnesses were similar among *Edmontosaurus* individuals (Fig. 3C). Hardness-based wear models for all three dinosaurs also wore to a morphology matching naturally worn batteries, including crests where enamel is absent and branched ridges (fig. S7).

In a phylogenetic context, these histological, biomechanical, and simulation data demonstrate how hadrosaurids evolved mammal-like grinding capacity. The primitive condition, in Hadrosauridae, seen in *Edmontosaurus* and most taxa (fig. S3), was a dual-function slicing-grinding system, presumably for the consumption of fibrous, moderately tough plants (*2*). The leading teeth have an inclined slicing plane, whereas all others form a file-like pavement. Highly wear-resistant enamel forms crests in all upper battery teeth but only in the lead teeth in the lower battery, because enamel was worn away before the teeth migrated across the chewing surface (Figs. 2A and 4A). Wear-resistant mantle dentine is the tissue that takes over the crest-forming role in the lower batteries (Fig. 4A and fig. S5). The inclined slicing faces in the leading teeth are composed of giant tubule curtains with intermediate wear resistance, spanning between the wear-resistant mantle dentine crests and the high-wear orthodentine basins (Fig. 2D and fig. S5). Large individual and branched giant tubules formed intermediate-height ridges partitioning the basins (Fig. 4A and fig. S5). Modeling shows that they influenced basin depth at each tooth position [greater sliding distance = greater scour (*23*)] and probably provided for finer grinding of plants than did major crests (fig. S5). Coronal cementum is prevalent, as in mammalian grinding teeth (Figs. 2D and 4A). It similarly served as a bridge minimizing stress singularities on the hard brittle crests, but also bound teeth together (fig. S5). Abscess-preventing secondary dentine is present only where the pulp cavity was locally breached and, unlike in mammalian grinding teeth, didn't substantially contribute to basin formation through wear.

The distribution of these characters phylogenetically shows that longitudinal giant tubules and secondary dentine evolved at the base of Ornithopoda, probably for abscess prevention in association with dental occlusion (fig. S3). Transverse giant tubules subsequently appeared in hadrosauroideans for steeper-angled slicing. The remaining tissues (mantle dentine and extensive coronal cementum) are primitive for Hadrosaurids and evolved as innovations for combined slicing and grinding (fig. S3). Tissue-complex modifications appear to have allowed for diversification into specialized ecological niches (fig. S3). Some taxa evolved teeth with coarse grinding pavements across the entire chewing area, presumably for processing tough plant matter (figs. S2 and S3). This was achieved through the loss of transversely oriented giant tubules, so slicing plane formation and basin partitioning couldn't occur. In other taxa, grinding capacity was completely lost and the teeth were specialized for high-angle slicing (fig. S3). In these batteries, transversely oriented giant tubules radiate throughout the teeth, so shearing faces formed at all wear stages across the chewing surfaces.

Hadrosaurids evolved the most histologically and biomechanically sophisticated dentitions known among reptiles, and these rivaled those of advanced herbivorous mammals in complexity. Three-dimensional tribological modeling allows for an improved understanding of tissue-level contributions to dental form and function. The ability to measure wear-relevant properties in fossils provides a new approach to study biomechanics throughout evolution. Such inferences will be enlightening across major mammalian and reptilian diversifications involving dental and dietary changes (*24*, *25*).

References and Notes

1. V. S. Williams, P. M. Barrett, M. A. Purnell, *Proc. Natl. Acad. Sci. U.S.A.* **106**, 11194 (2009).
2. J. S. Tweet, K. Chin, D. R. Braman, N. L. Murphy, *Palaios* **23**, 624 (2008).
3. R. S. Lull, N. E. Wright, *Spec. Pap. Geol. Soc. Am.* **40**, 1 (1942).
4. J. H. Ostrom, *Bull. Am. Mus. Nat. Hist.* **122**, 1 (1961).
5. D. B. Norman, D. B. Weishampel, in *Biomechanics in Evolution*, J. M. V. Rayner, R. J. Wootton, Eds. (Cambridge Univ. Press, Cambridge, 1991), pp. 161–181.
6. D. B. Weishampel, *Acta Palaeontol. Pol.* **28**, 271 (1983).
7. G. M. Erickson, *Proc. Natl. Acad. Sci. U.S.A.* **93**, 14623 (1996).
8. A. Prieto-Márquez, *Zool. J. Linn. Soc.* **159**, 435 (2010).
9. D. C. Evans, C. A. Forster, R. R. Reisz, in *Dinosaur Provincial Park: A Spectacular Ancient Ecosystem Revealed*, P. Currie, E. Koppelhus, Eds. (Indiana Univ. Press, Bloomington, IN, 2005), pp. 349–366.
10. B. Peyer, *Comparative Odontology* (Univ. of Chicago Press, Chicago, 1968).
11. S. Hillson, *Teeth* (Cambridge Univ. Press, Cambridge, 1986).
12. C. M. Janis, M. Fortelius, *Biol. Rev. Camb. Philos. Soc.* **63**, 197 (1988).
13. P. L. Lucas, *Dental Functional Morphology: How Teeth Work* (Cambridge Univ. Press, Cambridge, 2004).
14. W. J. Schmidt, A. Keil, *Polarizing Microscopy of Dental Tissues* (Pergamon Press, Oxford, 1971).
15. J. Leidy, *Smith. Contrib. Knowl.* **14**, 1 (1865).
16. R. J. Butler *et al*., *Proc. Biol. Sci.* **277**, 375 (2010).
17. Materials and methods are available as supporting materials on *Science* Online.
18. J. F. Archard, *J. Appl. Phys.* **24**, 981 (1953).
19. M. M. Khruschov, *Wear* **28**, 69 (1974).
20. J. D. Currey, R. M. Abeysekera, *Arch. Oral Biol.* **48**, 439 (2003).
21. W. M. Johnson, A. J. Rapoff, *J. Mater. Sci. Mater. Med.* **18**, 591 (2007).
22. W. G. Sawyer, *Tribol. Lett.* **17**, 139 (2004).
23. J. F. Archard, W. Hirst, *Proc. R. Soc. London Ser. A* **236**, 397 (1956).
24. K. Schwenk, Ed., *Feeding: Form, Function and Evolution in Tetrapod Vertebrates* (Academic Press, San Diego, CA, 2000).
25. R. R. Reisz, H. D. Sues, in *Evolution of Herbivory in Terrestrial Vertebrates: Perspectives from the Fossil Record,* H. D. Sues, Ed. (Cambridge Univ. Press, Cambridge, 2000), pp. 9–41.

Acknowledgments: We thank W. Nix, A. Prieto-Marquez, P. Lee, P. Druckenmiller, C. Taylor, and E. McCumiskey for their assistance and NSF (grant EAR 0959029 to G.M.E. and M.A.N.) for research funding. Data described in the paper are archived by the Computer Support Group of the Department of Biological Science at Florida State University as databases S1 to S19.

Supplementary Materials

www.sciencemag.org/cgi/content/full/338/6103/98/DC1
Materials and Methods
Supplementary Text
Figs. S1 to S7
Table S1
References (*26*–*40*)
Captions for Databases S1 to S19

9 May 2012; accepted 24 August 2012
10.1126/science.1224495

Rapid Acceleration Leads to Rapid Weakening in Earthquake-Like Laboratory Experiments

J. C. Chang,[1] D. A. Lockner,[2] Z. Reches[1]*

After nucleation, a large earthquake propagates as an expanding rupture front along a fault. This front activates countless fault patches that slip by consuming energy stored in Earth's crust. We simulated the slip of a fault patch by rapidly loading an experimental fault with energy stored in a spinning flywheel. The spontaneous evolution of strength, acceleration, and velocity indicates that our experiments are proxies of fault-patch behavior during earthquakes of moment magnitude (M_w) = 4 to 8. We show that seismically determined earthquake parameters (e.g., displacement, velocity, magnitude, or fracture energy) can be used to estimate the intensity of the energy release during an earthquake. Our experiments further indicate that high acceleration imposed by the earthquake's rupture front quickens dynamic weakening by intense wear of the fault zone.

Large earthquakes initiate at a small nucleation area and grow as propagating rupture fronts (*1*, *2*) (Fig. 1A). The propagating front activates a multitude of fault patches that undergo intense deformation (Fig. 1, B and C). Before the front arrives, the stress μ on each patch is generally lower than its static strength μ_s [both stress and strength are presented as the friction

Downloaded from www.sciencemag.org on July 5, 2013